Uniform Thin Films of CdSe and CdSe(ZnS) Core(Shell) Quantum Dots by Sol–Gel Assembly: Enabling Photoelectrochemical Characterization and Electronic Applications

Lasantha Korala,[†] Zhijie Wang,[‡] Yi Liu,[#] Stephen Maldonado,[‡] and Stephanie L. Brock[†,*]

[†]Department of Chemistry, Wayne State University, Detroit, Michigan 48202, United States , [‡]Chemistry Department, University of Michigan, Ann Arbor, Michigan 48109, United States , and [#]Electron Microscopy Facility, Oregon State University, Corvallis, Oregon 87331, United States

ABSTRACT Optoelectronic properties of quantum dot (QD) films are limited by (1) poor interfacial chemistry and (2) nonradiative recombination due to surface traps. To address these performance issues, sol–gel methods are applied to fabricate thin films of CdSe and core(shell) CdSe(ZnS) QDs. High-angle annular dark-field scanning transmission electron microscopy (HAADF-STEM) imaging with chemical analysis confirms that the surface of the QDs in the sol–gel thin films are chalcogen-rich, consistent with an oxidative-induced gelation mechanism in which connectivity is achieved by formation of dichalcogenide covalent linkages between particles. The ligand removal and assembly process is probed by thermogravimetric, spectroscopic, and microscopic studies. Further enhancement of interparticle coupling *via* mild thermal annealing, which removes residual ligands and reinforces QD connectivity, results in QD sol–gel thin films with superior charge transport properties, as shown by a dramatic enhancement of electrochemical photocurrent under white light illumination relative to thin films composed of ligand-capped QDs. A more than 2-fold enhancement in photocurrent, and a further increase in photovoltage can be achieved by passivation of surface defects *via* overcoating with a thin ZnS shell. The ability to tune interfacial and surface characteristics for the optimization of photophysical properties suggests that the sol–gel approach may enable formation of QD thin films suitable for a range of optoelectronic applications.

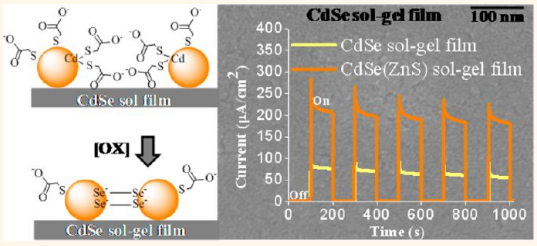

KEYWORDS: quantum dots · sol–gel methods · photocurrent · surface passivation · ligand exchange

Thin films of semiconductor quantum dots (QDs) are promising materials for electronic and optoelectronic device applications including field-effect transistors (FETs),[1,2] photodetectors,[3,4] light emitting diodes (LEDs)[5,6] and solar cells.[7,8] The size- and shape-tunable optical and electronic properties of QDs, along with their solution processability, permit great flexibility in device design, enabling the use of low cost fabrication methods such as solution coating[9,10] or printing.[11] The charge transport properties of QD thin films play a major role in device performance and depend on the extent of electronic coupling between neighboring QDs, where charge transport occurs by sequential tunneling.[12] Unfortunately, bulky organic ligands used in the synthesis of QDs reduce the interparticle coupling, and consequently have a destructive effect on the charge transport properties of QD films.

Reduction of the inter-QD spacing is one of the main strategies being investigated to improve the electronic communication between QDs in thin films. This can be done by removing the bulky organic surfactants by thermal annealing[13,14] or by exchanging them with smaller ligands, either in the solution phase before depositing the QDs as thin films (nitrosonium tetrafluoroborate,[15] molecular metal chalcogenides,[16–18] chalcogenide anions,[19,20] thiocyanate[21]) or in the solid phase after deposition (hydrazine,[22,13] NaOH,[23,24] thiols,[10,25–27] amines,[13,1] short-chain carboxylic acids[28]). Alternatively, sol–gel methods can be used to assemble metal chalcogenide QDs into gels, xerogels, and aerogels that have interconnected networks

* Address correspondence to sbrock@chem.wayne.edu.

Received for review October 2, 2012 and accepted January 25, 2013.

Published online January 25, 2013
10.1021/nn304563j

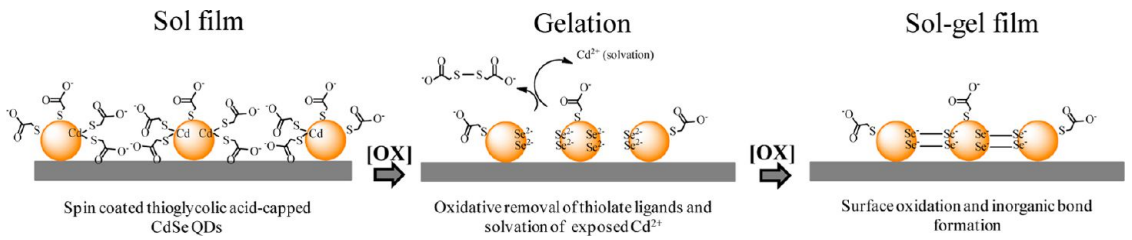

Scheme 1. Mechanism of oxidative ([OX]) gelation of a thioglycolic acid-capped QD film (sol film) submerged in a TNM solution.

of QDs.[29−31] This is achieved by oxidative decomplexation of thiolate capped QDs, exposing the particle and oxidizing surface chalcogenide species, resulting in interparticle linking *via* dichalcogenide bonding.[32] Recently, we took a major step toward practical exploitation of chalcogenide gels by fabricating transparent, micrometer-thick QD gel films that exhibited strong photoluminescence and high conductivities ($\sim 10^{-3}$ S·cm^{-1}).[33] However, the films were rough and we were unable to make crack-free thinner films by this approach. In the present work, we report a new strategy to fabricate high quality QD sol−gel thin films, and we evaluate the potential of these films for optoelectronic applications by means of photoelectrochemical measurements.

RESULTS AND DISCUSSION

CdSe QDs were synthesized according to modified literature procedures and capped with thiolate ligands.[34,35] Supporting Information, Figure S1 shows the UV−vis and PL spectra of purified trioctylphosphine oxide (TOPO)/stearic acid-capped QDs dispersed in toluene. According to the first excitonic peak in the absorption spectrum, CdSe QDs were determined to have diameters of ~5.3 nm.[36,37] After exchange with thiolate ligands, the bandgap remained unchanged, but the PL was almost completely quenched due to hole trapping at surface thiolates (Supporting Information, Figure S1).[38] The thiolate-capped QDs dispersed in methanol (sol) were then spin-coated onto substrates to form thin films of thiolate-capped QDs (sol films). Gelation was initiated by dipping the film into an oxidizing solution (tetranitromethane, TNM, in acetone). The films generated using mercaptoundecanoic acid (MUA) capping groups dissolved within a few seconds, indicating that the kinetics of gelation are not fast enough to overcome the redispersion of QDs in acetone. To increase the rate of oxidation of the thiolate ligands, the shorter chain ligand thioglycolic acid was used as the capping group. The short chain length is expected to afford easy accessibility of the oxidizing agent to the particle surface. Moreover, the shorter interparticle distances expected with thioglycolic acid as a ligand relative to MUA means the QDs will only have to migrate a short distance during the formation of interparticle bonds in the gelation process, which should prevent significant film cracking.

Spin-coated thioglycolic acid-capped QD films (sol films) (~70 nm thick) were immersed in solutions of TNM in acetone for one minute, followed by dipping in fresh methanol solution to remove the gelation byproducts (Scheme 1). In contrast to MUA-capped QDs, the thioglycolic acid-capped QD films (sol films) did not disperse in the acetone/TNM solution and the resultant sol−gel QD films were also insoluble in methanol, suggesting the kinetics of oxidation are fast enough to remove the polar capping groups on the surface of QDs, inducing gelation, and making the film insoluble in polar as well as nonpolar solvents. The films were subsequently annealed at 250 °C for 30 min. Supporting Information, Figure S2 shows TEM images of TOPO/stearic acid-capped QDs, and thioglycolic acid-capped QDs before and after the addition of TNM. The discrete particles have been "wired" into a network by the oxidative treatment.

We employed thermogravimetric analysis (TGA) to follow the ligand exchange, gelation, and annealing processes using bulk samples. The originally synthesized CdSe QDs contained large quantities of organic surfactants (TOPO/stearic acid) as indicated by a ~50% weight loss (Figure 1a). Successful exchange of the original organic ligands with thioglycolic acid was confirmed by the decrease of the weight loss down to ~13%, since thioglycolic acid has a much lower molecular weight than the original ligands (TOPO/stearic acid). Moreover, thermal decomposition starts around 220 °C for TOPO/stearic acid-capped QDs, but after thioglycolic acid exchange the loss starts at a much lower temperature, below 130 °C, indicative of a significant chemical change in the surface ligands. The gelation causes removal of surface thiolate ligands from the QD surface, and as a result, further decreases the weight loss experienced during TGA down to just ~8%.

These processes can also be followed by FTIR analysis. FTIR of a TOPO/stearic acid-capped QD film has a prominent peak in the C−H stretching region that virtually disappears upon exchange with the short-chain thioglycolic acid ligand (Supporting Information, Figure S3) consistent with a decrease in aliphatic hydrocarbon among the surface groups (*i.e.*, loss of TOPO, stearic acid capping groups). Loss of TOPO is further confirmed by the absence of a P═O stretching vibration peak in the thioglycolic acid-capped QD film (sol film). A small peak due to COO^- stretching is observed in both the TOPO/stearic acid film and the sol film, consistent with the presence of stearic acid in the former and thioglycolic acid in the latter. Overall,

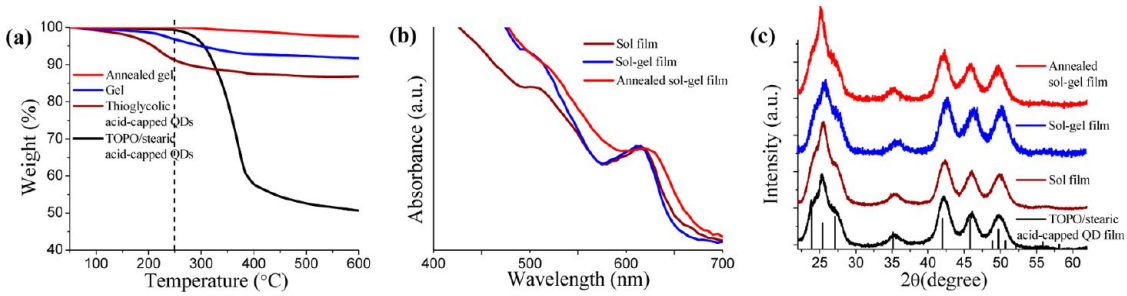

Figure 1. (a) Thermogravimetric scans of CdSe QDs before and after ligand exchange and a CdSe gel before and after annealing confirm the successful ligand exchange, loss of thiolate ligands during the gelation process, and removal of residual ligands in the annealing step. (b) UV−vis spectra of a thioglycolic acid-capped CdSe film before (sol film) and after gelation (sol−gel film), and after annealing the sol−gel film show that gelation causes minor surface etching of QDs (blue shift), and annealing results in greater QD−QD interaction (red shift). (c) XRD patterns of a TOPO/stearic acid-capped CdSe film, thioglycolic acid-capped CdSe film (sol-film), a sol−gel film, and an annealed sol−gel film indicate negligible changes in crystallite size during the ligand exchange, gelation, and annealing processes. The line diagram in panel c corresponds to bulk CdSe (from ISCD pattern PDF no. 77-2307).

the disappearance of C−H and P═O stretching while COO^- stretching is retained is consistent with the replacement of the bulky TOPO/stearic acid ligands with short chain thioglycolic acid.

The majority of the residual ligands are subject to decomposition at low temperatures (<250 °C) as indicated in Figure 1a where TGA analysis of an annealed gel (250 °C, 30 min) demonstrated only a 1−2% weight loss. This is important because a common problem with thermal treatment is that nanocrystals are not stable at the temperatures (>300 °C) needed to pyrolize commonly employed organic surfactants, and thus the QDs frequently sinter in this process and lose quantum confinement.[14] This is not the case for our materials, as evidenced by absorption spectra and X-ray diffraction patterns of films (Figure 1b,c). The absorption spectrum of a sol−gel film shows only a small blue shift of the first excitonic peak (5 nm, 17 meV) resulting from gelation. This may be due to surface etching during the gelation process. Removal of the thermally unstable residual ligands by annealing strengthens the connectivity of the QD network resulting in peak broadening and red shifting (10 nm, 33 meV) of the first excitonic peak relative to the sol−gel film. While this shift could be due to either the enhancement of interparticle coupling, crystallite growth, or a combination of these effects[39,40] a lack of change in the XRD peak breadths (which reflect crystallite size) suggests sintering is minimal. Thus, the major effect of the annealing step is to more effectively "wire" the particles into an interactive network.

Figure 2a shows photographs of sol−gel films before and after annealing. They appear crack-free, transparent and are visually identical. Microscopic evaluation of the films using FESEM reveal only nanoscale cracking of the film (Figure 2a−c) and AFM roughness measurements show the films (~70 nm thick) are smooth (roughness <2 nm) and uniform on the nanoscale (Figure 2d−f); no changes are observed during the gelation and annealing processes.

To evaluate the potential of sol−gel QD films for optoelectronic applications, we performed photoelectrochemical measurements using a three-electrode system comprising the QD film on ITO as the working electrode, a Pt-coil counter electrode and a saturated Ag/AgCl reference electrode. A 0.1 M polysulfide aqueous solution (Na_2S + NaOH + S) served as the electrolyte, and the photoresponse of TOPO/stearic acid-capped CdSe QD films (as-prepared) and CdSe sol−gel films (annealed at 250 °C) were studied under white light illumination (100 mW/cm^2).

The TOPO/stearic acid-capped CdSe QD films did not exhibit a detectable photocurrent, indicating poor charge transport that is likely due to the highly insulating nature of the bulky organic ligands. However, CdSe annealed sol−gel films displayed a ~75 μA cm^{-2} anodic photocurrent at −0.57 V (solution redox potential) with respect to the Ag/AgCl reference electrode, comparable to the only other report of photocurrent measurements on CdSe systems we could find in the literature ("bare" particle surfaces),[41] suggesting a significant improvement in charge transport arising from the interconnected QD network within the annealed sol−gel films (Figure 3). The rest potential of the annealed sol−gel films shifted from −0.65 to −1.00 V (*vs* Ag/AgCl) (Figure 3b, Supporting Information, Figure S4) upon introduction of light, consistent with intrinsic n-type doping in the films, which can also be shown in the rectifying shape of the *I*−*V* curve (Figure 3b). The enhanced communication between adjacent QDs enables the photogenerated electron carriers to travel to the ITO electrode efficiently while holes are captured by S^{2-} and transferred to the counter electrode; consequently, the recombination efficiency of the electron−hole at the QD surface is greatly reduced and photocurrent increases dramatically. There was a slight decrease of photocurrent at the beginning; however, as the systems have not yet been fully optimized, this is not unexpected. Stable photocurrents were observed after some time.

The promising photoresponse in the gel thin films can be rationalized by the linkage of QDs during the gelation process. As previously mentioned, treatment of thioglycolic acid-capped QD films (sol films) with

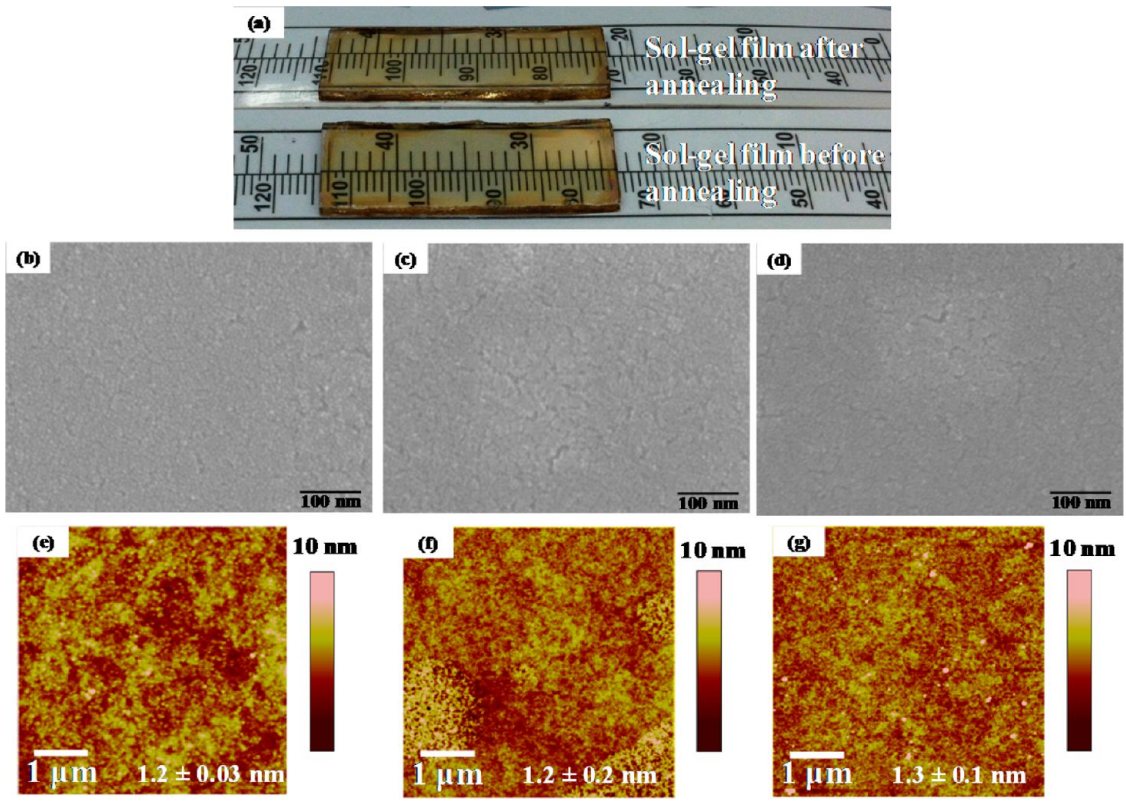

Figure 2. (a) Photographs of sol–gel films before and after annealing. FESEM images of a (b) thioglycolic acid-capped CdSe QD film (sol film) (c) sol–gel film, and (d) annealed sol–gel film. AFM images of a (e) thioglycolic acid-capped CdSe QD film (sol film) (f) sol–gel film, and (g) annealed sol–gel film. Both FESEM and AFM imaging confirm that there are no major morphological changes during the gelation and annealing processes.

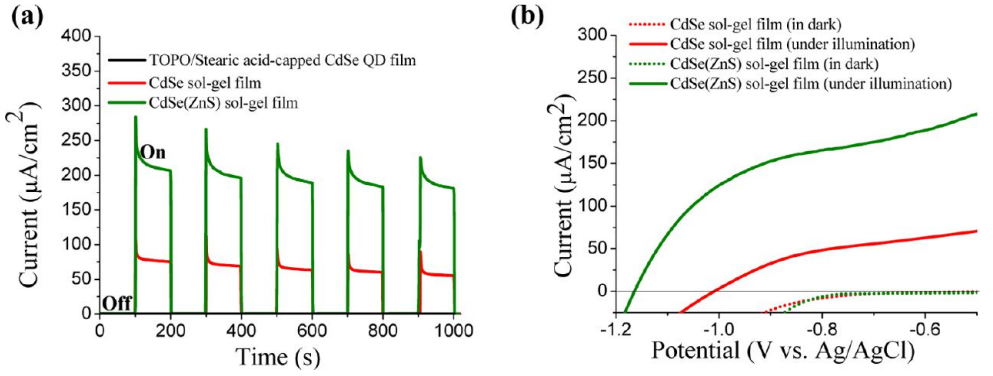

Figure 3. (a) Photocurrent response of a TOPO/stearic acid-capped CdSe QD film, and CdSe and CdSe(ZnS) sol–gel films (annealed at 250 °C), to chopped white light irradiation (100 mW/cm^2) at −0.57 V (solution redox potential) with respect to a Ag/AgCl reference electrode confirms the enhancement of charge transport properties in annealed sol–gel films. (b) *I*–*V* characteristics of the CdSe and CdSe(ZnS) sol–gel films (annealed at 250 °C). The ZnS shell leads to increased photocurrent, enhanced photovoltage, and sharper fill factor in annealed sol–gel films.

oxidant, TNM, removes surface thiolates and oxidizes the exposed chalcogenide on the QD surface, leading to dichalcogenide-bonded QDs.[32] In the case of CdSe QDs, removal of thiolate ligands causes solvation of exposed Cd^{2+} ions, and consequently, the Se^{2-}-rich QD surface can undergo further oxidation resulting in QDs linked by $(Se)_2^{2-}$ (Scheme 1). To confirm the Se rich interfaces between QDs in the gel relative to the surface of discrete QDs, we performed high-angle annular dark-field scanning TEM (HAADF-STEM) imaging with EDS elemental mapping using the ChemiSTEM technology developed by FEI.

Supporting Information, Figure S2 and Figure 4 show the HAADF images and EDS elemental mapping of TOPO/stearic acid-capped CdSe QDs, and thioglycolic acid-capped QDs gelled by treatment with TNM. The QDs are highly crystalline and have significant Cd (blue) and Se (red) signal throughout. In contrast, the signal for gelled particles is dominated by Se, which is continuous throughout the interconnected network,

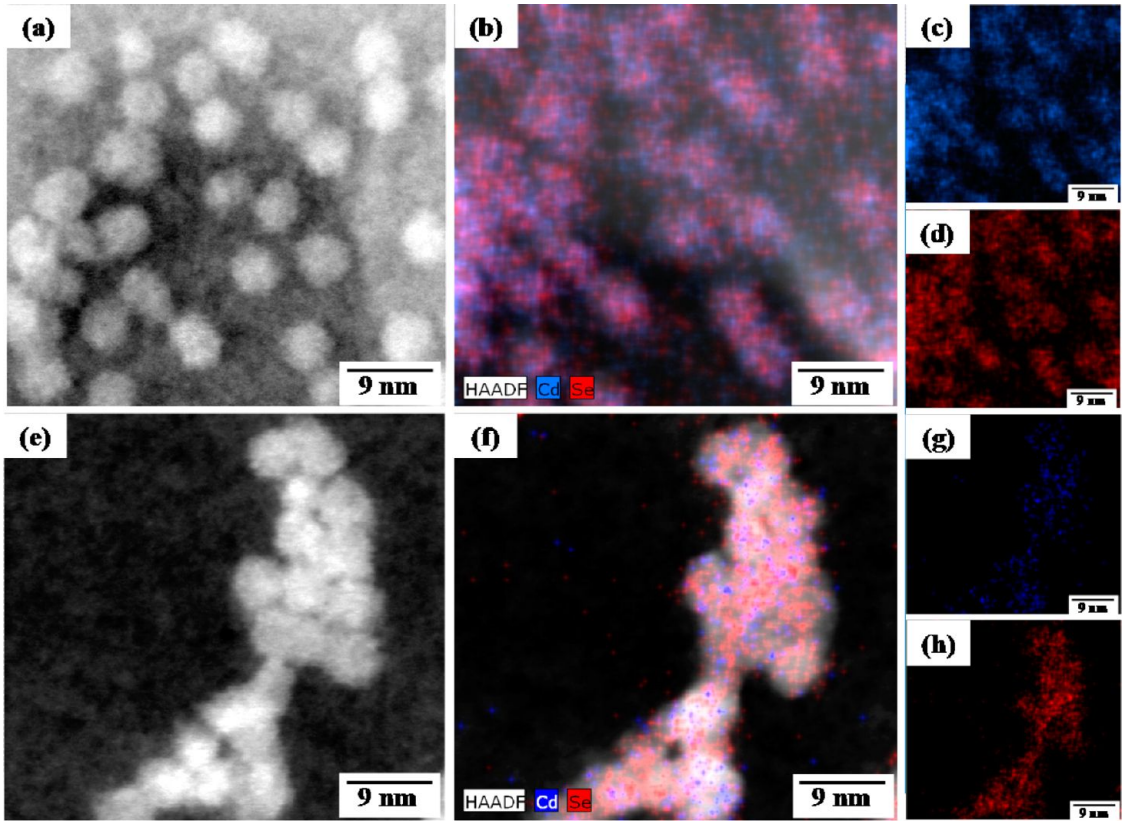

Figure 4. (a) A HAADF-STEM image of TOPO/stearic acid-capped CdSe QDs, and (b−d) EDS elemental mapping for Cd and Se. (e) A HAADF-STEM image of thioglycolic acid-capped CdSe QDs after gelation, and (f−h) EDS elemental mapping for Cd and Se. The distinct increase in Se signal relative to Cd in gelled QDs relative to TOPO/stearic acid-capped QDs is consistent with the proposed mechanism of gelation.

consistent with Se-mediated interparticle bonding. The deficiency in Cd in the gelled network relative to the starting particles is particularly evident when Figure 4 images c and g are compared.

We next sought to explore the effect of passivation of the CdSe surface on the photoconductivity of the films, considering the fact that surface modification during the ligand exchange, gelation, and annealing processes could lead to defect-related recombination. Nonradiative recombination can be suppressed by passivating the surface states of the chromophore (CdSe) by growth of a shell consisting of a material with a larger band gap, ZnS.[42] Although Type-I band alignment, as occurs when the valence band and conduction band of the core are sandwiched by those of the shell, which is the case for CdSe(ZnS), does not favor exciton dissociation, several reports have shown that enhancement of the photocurrent for QD-sensitized solar cells is realized when fabricated using CdSe(ZnS) core(shell) QDs.[43,44] Moreover, Zhu and co-workers have observed that the charge separation rate in CdSe(ZnS) QDs depends on the shell thickness, with an exponential decrease in the charge separation kinetics with increasing ZnS shell thickness.[36] Thus, in order to improve surface passivation without overly compromising charge separation, we overcoated the core CdSe QDs with a thin shell of ZnS (~1−2 monolayers).

ZnS was grown on CdSe cores by slowly injecting a mixture of diethyl zinc and bis(trimethylsilyl)sulfide as zinc and sulfur precursors.[45] Supporting Information, Figure S6 shows the UV−vis and PL spectra of core and core(shell) QDs dispersed in toluene. The significant enhancement in band-edge PL intensity upon overcoating is consistent with a reduction of hole traps on the QD surface. The subsequent gelation and annealing processes have a large effect on the optical properties; the PL intensity decreases upon gelation and is almost completely quenched after annealing. PL quenching can be attributed to formation of surface trap states or generation of free charge carriers due to the enhancement of electronic coupling.[20,25] Because of the surface passivation provided by the thin shell of ZnS, the contribution from the latter to the PL quenching should be significant. Consistent with a hypothesis of decreased surface trapping giving rise to increased free charge carriers, a more than 2-fold increase of photocurrent (Figure 3a) and higher optical conversion quantum yield (Supporting Information, Figure S8) were observed for annealed core(shell) sol−gel films compared to the corresponding CdSe-only films The notion that the presence of a ZnS shell decreased surface trapping as a major recombination pathway is also supported by the measured change in rest potential on moving from dark to illuminated conditions (Supporting

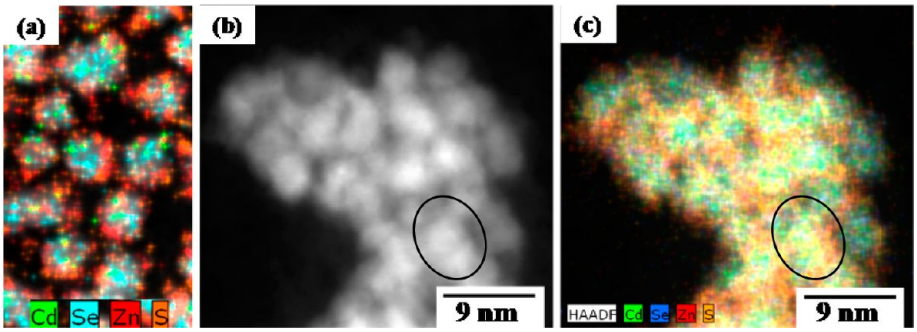

Figure 5. (a) EDS elemental mapping of TOPO/stearic acid-capped CdSe(ZnS) QDs for Cd, Se, Zn, and S shows that the CdSe cores are only partially covered by the ZnS shell. (b) A HAADF-STEM image of thioglycolic acid-capped CdSe(ZnS) QDs after gelation, and (c) EDS elemental mapping for Cd, Se, Zn and S in CdSe(ZnS) gels. The circled area shows one of several places where there appears to be direct contact between CdSe cores.

Information, Figure S4). At steady-state, the attainable photovoltage (*i.e.*, the difference between the rest potential in the dark and under illumination) of a photoelectrode is a measure of the ratio of the product of charge carrier concentrations under illumination to the product of charge carrier concentrations in the dark,

$$\Delta V = \frac{kT}{q} \ln\left(\frac{np}{n_i^2}\right)$$

where ΔV is the difference in rest potentials in the dark and under illumination, k is Boltzmann's constant, T is temperature, q is the unsigned charge of an electron, n is the steady-state electron concentration, p is the steady-state hole concentration, and n_i is the intrinsic concentration of carriers in the semiconductor. All recombination processes act to minimize n and p under illumination. The larger measured change in rest potential for the ZnS-coated CdSe sol–gel film as compared to the bare CdSe sol–gel film under the same illumination conditions implies a larger population imbalance and, accordingly, a decreased rate of total recombination. The increased net anodic photocurrents for the ZnS-coated CdSe sol–gel films also imply sufficiently fast hole transfer through the ZnS shell. Quenching experiments with CdSe(ZnS) core(shell) quantum dots have previously demonstrated that strong coupling of a CdSe core with acceptors/donors on the opposite side of the thin ZnS shell (<5 monolayers) allows rapid charge transfer.[46,47] Accordingly, we posit that the thinness of the ZnS layer reduces trap sites where recombination can occur while enabling strong electronic coupling between the CdSe core and the dissolved solution redox mediator. This leads to improvement of all aspects of the photoresponse of annealed CdSe–ZnS core–shell sol–gel films relative to the corresponding CdSe sol–gel films, as reflected in Figure 3b; that is, increased photocurrent, enhanced photovoltage, and sharper fill factor.

Elemental mapping of the CdSe(ZnS) core(shell) QDs and sol–gel network (Figure 5) supports our hypothesis for the enhanced performance of core(shell) sol–gel films relative to CdSe sol–gel films. As shown in Figure 5a, the CdSe core is only partially covered by the ZnS shell. Because of these imperfections in the ZnS shell, the CdSe cores have points of direct contact within the network that is created by the oxidative gelation process (Figure 5b,c). The decrease of defect-related recombination by partial passivation of the surface states that is achieved by growing a thin shell of ZnS, combined with direct contact of CdSe cores through defects in the shell[43] may collectively contribute to the enhancement of photocurrent for the CdSe(ZnS) core(shell) sol–gel films relative to CdSe films.

CONCLUSIONS

We have developed a new method to fabricate high quality CdSe QD sol–gel films by applying gelation strategies to spin-coated thioglycolic acid-capped QD films (sol films). This method enables improved charge transport properties in QD solids by enhancing interparticle coupling *via* formation of oxidation-induced dichalcogenide linkages. Overcoating CdSe QDs with a thin ZnS shell reduces unpassivated surface states, and thus charge-trapping, and results in a more than 2-fold increase of photocurrent. The ability to tune interfacial and surface characteristics for the optimization of photophysical properties suggests the sol–gel approach may yield QD thin films suitable for a range of optoelectronic applications.

METHODS

Synthesis of CdSe and CdSe(ZnS) Core(Shell) QDs and Thiolate Exchange. CdSe and CdSe(ZnS) core(shell) quantum dots (QDs) were synthesized following literature procedures, with modifications (Supporting Information), and exchanged with thiolate ligands.[34,35]

Deposition of CdSe and CdSe(ZnS) Sol–Gel Thin Films (~70 nm Thick). Glass slides or silicon wafers were used as substrates for film deposition. Substrates were sonicated in acetone, ethanol, and water, respectively, for 15 min each. After rinsing with distilled water, substrates were dried under nitrogen gas blow. QD sols were spin coated

(4000 rpm, 40 s) on glass or silicon substrates and dipped in TNM solution (50 μL of 3% TNM in 10 mL of acetone) for one minute and then dipped in fresh methanol solution for several minutes to remove the gelation byproducts (2 times) and finally dried under ambient conditions. For photocurrent measurements, QD sols were spin coated (4000 rpm, 40 s) on ITO-coated glass substrates (Delta Technologies, R_s = 5−15 Ω) and gelled following the above procedure. ITO substrates were cleaned following the same procedure as for the glass substrates. Prior to spin coating, a portion of the ITO-coated glass substrate on one side was covered with tape to ensure a bare ITO region without QD film. After spin coating, films were dried in ambient conditions and then annealed at 250 °C for 30 min under argon flow.

Characterization. *X-ray Diffraction (XRD).* XRD was performed on a Rigaku Diffractometer (RU200B) using the Kα line of a Cu rotating anode source (40 kV, 150 mA). Films were deposited on silicon substrates for the XRD analysis.

Transmission Electron Microscopy (TEM). TEM and energy dispersive spectroscopy (EDS) were carried out on a JEOL 2010 transmission electron microscope operated at an accelerating voltage of 200 kV with a coupled EDS detector (EDAX, Inc.). To image the QDs before and after gelation, a thioglycolic acid-capped QD sol was drop cast onto a carbon-coated copper TEM grid and then dipped in a TNM solution (50 μL of 3% TNM in 10 mL of acetone) for one minute and then submerged in fresh methanol solution for several minutes before allowing to air-dry.

Scanning Transmission Electron Microscopy (STEM). High resolution images were taken using the FEI Titan 80−200 scanning transmission electron microscope (S/TEM) operated at 200 kV. In STEM mode, *Z*-contrast images were taken using a high-angle annular dark-field (HAADF) detector (Fischione Instruments), and elemental mapping was performed using the "Super X" Energy Dispersive Spectrometric (EDS) system, which consists of four windowless silicon-drift detectors (SDD) positioned symmetrically around the specimen in a unique FEI design. The detectors are made by PN Sensors, utilizing a pulse processor from Bruker Corporation. The integration of Super X EDS detection in combination with the high-brightness electron source is also called ChemiSTEM Technology, introduced by the FEI company in 2010. Samples were prepared as described in the section on transmission electron microscopy.

Field Emission Scanning Electron Microscopy (FESEM). FESEM images were obtained using a JEOL JSM-7600F field emission scanning electron microscope operated at an accelerating voltage of 15 kV in high-vacuum mode. Films were deposited on ITO substrates.

Atomic Force Microscopy (AFM). AFM was performed using a Dimension 3100 AFM (VEECO) in tapping mode. Films were deposited on glass substrates. The surface roughness was measured by using the roughness command (Nanoscope) from three areas on the film of 5 × 5 μm^2 each. The film was then scratched carefully with a blade. The film thickness was determined using the sectional height analysis command (Nanoscope) by measuring the depth of the scratch at five locations on the film.

Photoluminescence and UV−vis Spectroscopy. PL (excitation wavelength, 480 nm) and UV−vis spectra were obtained with a Cary Eclipse (Varian, Inc.) fluorescence spectrometer and a Cary 50 (Varian Inc.) spectrometer. Films were deposited on glass substrates for the PL and UV−vis spectroscopy.

FT-IR Spectroscopy. FT-IR spectra were obtained using a Bruker TENSOR 27 FT-IR spectrometer (Bruker Optics, inc.). Films were deposited on both glass (spin-casting) and silicon substrates (drop casting) and spectra were recorded in transmission mode (glass substrate) and reflectance mode (silicon substrate). Transmission IR spectra were intensity normalized to the absorbance of the first excitonic peak in the absorption spectrum. Reflectance IR spectra were acquired on films deposited from QD solutions (TOPO/stearic acid- and thioglycolic acid-capped) with similar particle concentration.

Thermogravimetric Analysis (TGA). TGA measurements were performed on a Perkin-Elmer, Pyris 1 TGA under nitrogen flow. The temperature of the samples (∼10 mg) was increased up to 600 °C at a rate of 10 °C/min.

Photoelectrochemical Measurements. Photocurrent measurements were performed using a Schlumberger 1286 potentiostat in a three-electrode configuration with a Pt-coil counter electrode and a saturated Ag/AgCl reference electrode. CdSe and CdSe-(ZnS) QD films (TOPO/stearic acid-capped QD films and annealed sol−gel films) fabricated on ITO-coated glass were used as working electrodes. The concentration of the TOPO/stearic acid-capped QD solution was adjusted to fabricate films with approximately similar absorbance values to the sol−gel films. The bare ITO region was mounted onto a coiled tinned copper wire using conductive silver paste (GC electronics) and sealed with Hysol 1C epoxy. The photoactive area was determined by optical image analysis. The electrodes were placed in a Teflon cell (with a glass window for light illumination) containing a 0.1 M polysulfide aqueous solution (Na_2S + NaOH + S) as electrolyte. White light illumination was provided by a tungsten halogen lamp light source (ELH, Osram) with a quartz diffuser. The illumination intensity was set to 100 mW/cm^2 using a thermopile (S302A, Thorlabs), and photocurrent measurements were performed at −0.57 V (solution redox potential) with respect to the Ag/AgCl reference electrode. No external bias was applied.

Quantum efficiency measurements were obtained with an Oriel 150 W Xe arc lamp (Newport) and a quarter-turn single-grating monochromator (Newport). Sample measurements were recorded with chopped illumination (20 Hz), and a quartz beam splitter was used to simultaneously record the light output intensity with a separate Si photodiode (Newport) to adjust for fluctuations in lamp intensity. Absolute photocurrents were measured by a digital PAR 273 potentiostat at −0.57 V with respect to the Ag/AgCl reference electrode, and the output current signal was connected to a Stanford Instruments SR830 lock-in amplifier. The output signals from the lock-in amplifier and the reference Si photodiode were fed into a computer controlled by custom-written LabVIEW software.

Conflict of Interest: The authors declare no competing financial interest.

Supporting Information Available: Materials, details of the synthesis of QDs, ligand exchange, additional UV−vis, PL and IR spectra, TEM images, rest potential response and quantum efficiency measurements of films. This material is available free of charge *via* the Internet at http://pubs.acs.org.

Acknowledgment. L.K. and S.B. thank the National Institutes of Health, National Cancer Institute (R44 CA138013-03, *via* a subcontract from Weinberg Medical Physics, LLC), and Z. W. and S.M. thank the National Science Foundation (DMR-1054303), for support of this work. We thank Li Li for providing AFM imaging data and Guangzhao Mao for use of the AFM instrument (WSU, Chemical Engineering). FESEM data were acquired on a JEOL JSM-7600F purchased in part from funds provided by NSF MRI award 0922912, and HAADF/STEM data were acquired on an FEI Titan 80-200 field emission transmission electron microscope with ChemiSTEM technology purchased in part from funds provided by NSF MRI award 1040588 and Oregon Nanoscience and Microtechnologies Institute (ONAMI).

REFERENCES AND NOTES

1. Yu, D.; Wang, C.; Guyot-Sionnest, P. *n*-Type Conducting CdSe Nanocrystal Solids. *Science* **2003**, *300*, 1277–1280.
2. Ridley, B. A.; Nivi, B.; Jacobson, J. M. All-Inorganic Field Effect Transistors Fabricated by Printing. *Science* **1999**, *286*, 746–749.
3. Oertel, D. C.; Bawendi, M. G.; Arango, A. C.; Bulovic, V. Photodetectors Based on Treated CdSe Quantum-Dot Films. *Appl. Phys. Lett.* **2005**, *87*, 213505.
4. Konstantatos, G.; Howard, I.; Fischer, A.; Hoogland, S.; Clifford, J.; Klem, E.; Levina, L.; Sargent, E. H. Ultrasensitive Solution-Cast Quantum Dot Photodetectors. *Nature* **2006**, *442*, 180–183.
5. Colvin, V. L.; Schlamp, M. C.; Alivisatos, A. P. Light-Emitting Diodes Made from Cadmium Selenide Nanocrystals and a Semiconducting Polymer. *Nature* **1994**, *370*, 354–357.
6. Coe, S.; Woo, W.-K.; Bawendi, M.; Bulovic, V. Electroluminescence from Single Monolayers of Nanocrystals in Molecular Organic Devices. *Nature* **2002**, *420*, 800–803.

7. Gur, I.; Fromer, N. A.; Geier, M. L.; Alivisatos, A. P. Air-Stable All-Inorganic Nanocrystal Solar Cells Processed from Solution. *Science* **2005**, *310*, 462–465.
8. Huynh, W. U.; Dittmer, J. J.; Alivisatos, A. P. Hybrid Nanorod-Polymer Solar Cells. *Science* **2002**, *295*, 2425–2427.
9. Akhavan, V. A.; Goodfellow, B. W.; Panthani, M. G.; Reid, D. K.; Hellebusch, D. J.; Adachi, T.; Korgel, B. A. Spray-Deposited $CuInSe_2$ Nanocrystal Photovoltaics. *Energy Environ. Sci.* **2010**, *3*, 1600–1606.
10. Luther, J. M.; Law, M.; Song, Q.; Perkins, C. L.; Beard, M. C.; Nozik, A. J. Structural, Optical, and Electrical Properties of Self-Assembled Films of PbSe Nanocrystals Treated with 1,2-Ethanedithiol. *ACS Nano* **2008**, *2*, 271–280.
11. Haverinen, H. M.; Myllyla, R. A.; Jabbour, G. E. Inkjet Printing of Light Emitting Quantum Dots. *Appl. Phys. Lett.* **2009**, *94*, 073108.
12. Vanmaekelbergh, D.; Liljeroth, P. Electron-Conducting Quantum Dot Solids: Novel Materials Based on Colloidal Semiconductor Nanocrystals. *Chem. Soc. Rev.* **2005**, *34*, 299–312.
13. Law, M.; Luther, J. M.; Song, Q.; Hughes, B. K.; Perkins, C. L.; Nozik, A. J. Structural, Optical, and Electrical Properties of PbSe Nanocrystal Solids Treated Thermally or with Simple Amines. *J. Am. Chem. Soc.* **2008**, *130*, 5974–5985.
14. Drndic, M.; Jarosz, M. V.; Morgan, N. Y.; Kastner, M. A.; Bawendi, M. G. Transport Properties of Annealed CdSe Colloidal Nanocrystal Solids. *J. Appl. Phys.* **2002**, *92*, 7498–7503.
15. Dong, A.; Ye, X.; Chen, J.; Kang, Y.; Gordon, T.; Kikkawa, J. M.; Murray, C. B. A Generalized Ligand-Exchange Strategy Enabling Sequential Surface Functionalization of Colloidal Nanocrystals. *J. Am. Chem. Soc.* **2010**, *133*, 998–1006.
16. Kovalenko, M. V.; Scheele, M.; Talapin, D. V. Colloidal Nanocrystals with Molecular Metal Chalcogenide Surface Ligands. *Science* **2009**, *324*, 1417–1420.
17. Lee, J.-S.; Kovalenko, M. V.; Huang, J.; Chung, D. S.; Talapin, D. V. Band-like Transport, High Electron Mobility and High Photoconductivity in All-Inorganic Nanocrystal Arrays. *Nat. Nanotechnol.* **2011**, *6*, 348–352.
18. Kovalenko, M. V.; Bodnarchuk, M. I.; Zaumseil, J.; Lee, J.-S.; Talapin, D. V. Expanding the Chemical Versatility of Colloidal Nanocrystals Capped with Molecular Metal Chalcogenide Ligands. *J. Am. Chem. Soc.* **2010**, *132*, 10085–10092.
19. Nag, A.; Kovalenko, M. V.; Lee, J.-S.; Liu, W.; Spokoyny, B.; Talapin, D. V. Metal-free Inorganic Ligands for Colloidal Nanocrystals: S^{2-}, HS^-, Se^{2-}, HSe^-, Te^{2-}, HTe^-, TeS_3^{2-}, OH^-, and NH_2^- as Surface Ligands. *J. Am. Chem. Soc.* **2011**, *133*, 10612–10620.
20. Zhang, H.; Hu, B.; Sun, L.; Hovden, R.; Wise, F. W.; Muller, D. A.; Robinson, R. D. Surfactant Ligand Removal and Rational Fabrication of Inorganically Connected Quantum Dots. *Nano Lett.* **2011**, *11*, 5356–5361.
21. Fafarman, A. T.; Koh, W.-k.; Diroll, B. T.; Kim, D. K.; Ko, D.-K.; Oh, S. J.; Ye, X.; Doan-Nguyen, V.; Crump, M. R.; Reifsnyder, D. C.; *et al.* Thiocyanate-Capped Nanocrystal Colloids: Vibrational Reporter of Surface Chemistry and Solution-Based Route to Enhanced Coupling in Nanocrystal Solids. *J. Am. Chem. Soc.* **2011**, *133*, 15753–15761.
22. Talapin, D. V.; Murray, C. B. PbSe Nanocrystal Solids for *n*- and *p*-Channel Thin Film Field-Effect Transistors. *Science* **2005**, *310*, 86–89.
23. Yu, D.; Wehrenberg, B. L.; Jha, P.; Ma, J.; Guyot-Sionnest, P. Electronic Transport of *n*-type CdSe Quantum Dot Films: Effect of Film Treatment. *J. Appl. Phys.* **2006**, *99*, 104315.
24. Jarosz, M. V.; Porter, V. J.; Fisher, B. R.; Kastner, M. A.; Bawendi, M. G. Photoconductivity Studies of Treated CdSe Quantum Dot Films Exhibiting Increased Exciton Ionization Efficiency. *Phys. Rev. B* **2004**, *70*, 195327.
25. Talgorn, E.; Moysidou, E.; Abellon, R. D.; Savenije, T. J.; Goossens, A.; Houtepen, A. J.; Siebbeles, L. D. A. Highly Photoconductive CdSe Quantum-Dot Films: Influence of Capping Molecules and Film Preparation Procedure. *J. Phys. Chem. C* **2010**, *114*, 3441–3447.
26. Klem, E. J. D.; Shukla, H.; Hinds, S.; MacNeil, D. D.; Levina, L.; Sargent, E. H. Impact of Dithiol Treatment and Air Annealing on the Conductivity, Mobility, and Hole Density in PbS Colloidal Quantum Dot Solids. *Appl. Phys. Lett.* **2008**, *92*, 212105.
27. Lefrancois, A.; Couderc, E.; Faure-Vincent, J.; Sadki, S.; Pron, A.; Reiss, P. Effect of the Treatment with (Di-)amines and Dithiols on the Spectroscopic, Electrochemical and Electrical Properties of CdSe Nanocrystals' Thin Films. *J. Mater. Chem.* **2011**, *21*, 11524–11531.
28. Zarghami, M. H.; Liu, Y.; Gibbs, M.; Gebremichael, E.; Webster, C.; Law, M. p-Type PbSe and PbS Quantum Dot Solids Prepared with Short-Chain Acids and Diacids. *ACS Nano* **2010**, *4*, 2475–2485.
29. Arachchige, I. U.; Brock, S. L. Sol−Gel Assembly of CdSe Nanoparticles to Form Porous Aerogel Networks. *J. Am. Chem. Soc.* **2006**, *128*, 7964–7971.
30. Arachchige, I. U.; Brock, S. L. Highly Luminescent Quantum-Dot Monoliths. *J. Am. Chem. Soc.* **2007**, *129*, 1840–1841.
31. Mohanan, J. L.; Arachchige, I. U.; Brock, S. L. Porous Semiconductor Chalcogenide Aerogels. *Science* **2005**, *307*, 397–400.
32. Pala, I. R.; Arachchige, I. U.; Georgiev, D. G.; Brock, S. L. Reversible Gelation of II−VI Nanocrystals: The Nature of Interparticle Bonding and the Origin of Nanocrystal Photochemical Instability. *Angew. Chem., Int. Ed.* **2010**, *122*, 3743–3747.
33. Korala, L.; Li, L.; Brock, S. L. Transparent Conducting Films of CdSe(ZnS) Core(shell) Quantum Dot Xerogels. *Chem. Commun.* **2012**, *48*, 8523–8525.
34. Qu, L.; Peng, X. Control of Photoluminescence Properties of CdSe Nanocrystals in Growth. *J. Am. Chem. Soc.* **2002**, *124*, 2049–2055.
35. Hines, M. A.; Guyot-Sionnest, P. Synthesis and Characterization of Strongly Luminescing ZnS-Capped CdSe Nanocrystals. *J. Phys. Chem. Lett.* **1996**, *100*, 468–471.
36. Jasieniak, J.; Smith, L.; Embden, J. v.; Mulvaney, P.; Califano, M. Re-examination of the Size-Dependent Absorption Properties of CdSe Quantum Dots. *J. Phys. Chem. C* **2009**, *113*, 19468–19474.
37. Yu, W. W.; Qu, L.; Guo, W.; Peng, X. Experimental Determination of the Extinction Coefficient of CdTe, CdSe, and CdS Nanocrystals. *Chem. Mater.* **2003**, *15*, 2854–2860.
38. Wuister, S. F.; de Mello Donegá, C.; Meijerink, A. Influence of Thiol Capping on the Exciton Luminescence and Decay Kinetics of CdTe and CdSe Quantum Dots. *J. Phys. Chem. B* **2004**, *108*, 17393–17397.
39. Williams, K. J.; Tisdale, W. A.; Leschkies, K. S.; Haugstad, G.; Norris, D. J.; Aydil, E. S.; Zhu, X. Y. Strong Electronic Coupling in Two-Dimensional Assemblies of Colloidal PbSe Quantum Dots. *ACS Nano* **2009**, *3*, 1532–1538.
40. Artemyev, M. V.; Woggon, U.; Jaschinski, H.; Gurinovich, L. I.; Gaponenko, S. V. Spectroscopic Study of Electronic States in an Ensemble of Close-Packed CdSe Nanocrystals. *J. Phys. Chem. B* **2000**, *104*, 11617–11621.
41. Webber, D. H.; Brutchey, R. L. Ligand Exchange on Colloidal CdSe Nanocrystals Using Thermally Labile *tert*-Butylthiol for Improved Photocurrent in Nanocrystal Films. *J. Am. Chem. Soc.* **2011**, *134*, 1085–1092.
42. Porter, V. J.; Geyer, S.; Halpert, J. E.; Kastner, M. A.; Bawendi, M. G. Photoconduction in Annealed and Chemically Treated CdSe/ZnS Inorganic Nanocrystal Films. *J. Phys. Chem. C* **2008**, *112*, 2308–2316.
43. Sambur, J. B.; Parkinson, B. A. CdSe/ZnS Core/Shell Quantum Dot Sensitization of Low Index TiO_2 Single Crystal Surfaces. *J. Am. Chem. Soc.* **2010**, *132*, 2130–2131.
44. Shen, Q.; Kobayashi, J.; Diguna, L. J.; Toyoda, T. Effect of ZnS Coating on the Photovoltaic Properties of CdSe Quantum Dot-Sensitized Solar Cells. *J. Appl. Phys.* **2008**, *103*, 084304–5.
45. Hines, M. A.; Guyot-Sionnest, P. Synthesis and Characterization of Strongly Luminescing ZnS-Capped CdSe Nanocrystals. *J. Phys. Chem.* **1996**, *100*, 468–471.

46. Dias, E. A.; Sewall, S. L.; Kambhampati, P. Light Harvesting and Carrier Transport in Core/Barrier/Shell Semiconductor Nanocrystals. *J. Phys. Chem. C* **2006**, *111*, 708–713.
47. Makhal, A.; Yan, H.; Lemmens, P.; Pal, S. K. Light Harvesting Semiconductor Core−Shell Nanocrystals: Ultrafast Charge Transport Dynamics of CdSe−ZnS Quantum Dots. *J. Phys. Chem. C* **2009**, *114*, 627–632.